Experimental and numerical analysis of the influence of intramedullary nail position on the cut-out phenomenon.

Arias-Blanco A.[1], Marco M.[1,*], Giner E.[2], Larraínzar-Garijo R.[3], Miguélez M.H. [1]

[1] Department of Mechanical Engineering, Universidad Carlos III de Madrid, Spain.

[2] Institute of Mechanical and Biomechanical Engineering (I2MB), Department of Mechanical and Materials Engineering, Universitat Politècnica de València, Spain.

[3]Service of Orthopaedic Surgery and Traumatology, University Hospital Infanta Leonor, Universidad Complutense de Madrid, Spain.

Abstract:

Background and objective: Proximal femur fractures, colloquially known as hip fractures, are a common pathology with increasing incidence in the last years due to the enhanced ageing population. Regarding the extracapsular fracture, the treatment for this pathology consists of a fixation of the fragments using an osteosynthesis device, mainly the intramedullary nail. This repairing method implies several complications, which may include the failure of the fixation device, frequently occurring due to the "cut-out" mechanism. The present work focuses on the study of how the position of the cephalic screw, which should be fixed during surgery, affects the cut-out risk. Through experimental tests and numerical models some variables that can be critical for the cut-out phenomenon are analysed.

Methods: This study has been carried out through a numerical model based on the finite element method and experimental tests. The digital image correlation technique has been used in experimental tests to measure displacements on the femoral surface with the objective of numerical model validation. Some basic daily activities with different intramedullary nail positions have been analysed through the numerical model, considering variables that can induce the cut-out complication.

Results: The results show how the intramedullary nail position clearly influences the cut-out risk, showing that displacements in the upper, anterior and posterior direction increase the cut-out risk, while displacement in the lower direction endangers the intramedullary nail itself. Thus, the centred position is the one which reduces the cut-out risk.

Conclusions: This work supposes an improvement in the knowledge of the cut-out phenomenon thanks to the combination of experimental testing and validated numerical models. The effects of different intramedullary nail positions in the femoral head are studied, including a novelty variable as torque, which is critical for the structural integrity of the fixation. The main conclusion of the work is the determination of the central intramedullary nail position as the most favourable one for decreasing the cut-out risk.

Keywords: Hip fracture; Extracapsular fracture; Intramedullary nail; Cut-out; Digital Image Correlation; Finite Element Method.

*Corresponding author:
E-mail address: mimarcoe@ing.uc3m.es (M. Marco)

1. Introduction.

Proximal fractures of the femur are a severe health problem in nowadays society. This increment is explained mainly due to the improvement of life expectancy in the recent years, thus increasing the elderly population and, therefore, the related diseases. This is why this kind of pathologies is more common in advanced countries, with a global increase in the total number of hip fractures [1].

In addition to the large number of cases, it is worth noting the elevated mortality rate of 4.71-5.85% (25-33% one year after the intervention) [2] and the fact that one in five patients will need permanent socio-sanitary care [3]. An in-depth study and the improvement of the treatment of proximal femur fractures are still a challenge.

Once the fracture has occurred, there are two main types of proximal femur fractures: intracapsular and extracapsular fractures [4], representing each one around 50% of the cases [5], [6]. The usual treatment of extracapsular fractures consists of internal fixation of the fragments using different osteosynthesis devices, including intramedullary nails. These mechanical fixations imply several complications that could appear after the intervention. Two main phenomena may lead to the failure of the fixation devices [7]: the mechanical failure of the fixation device itself and the so-called cut-out. The latter is the problem addressed in this work and is defined as the collapse of the femoral neck. It implies an oblique displacement and/or rotation of the femoral head, thus causing damage to the trabecular bone and leading to the relative displacement of the cephalic screw with respect to the femoral head [8]. An example of a cut-out failure is shown in **Fig. 1**, although in this case it could also be induced by an incorrect reduction of the fracture.

1. Introduction

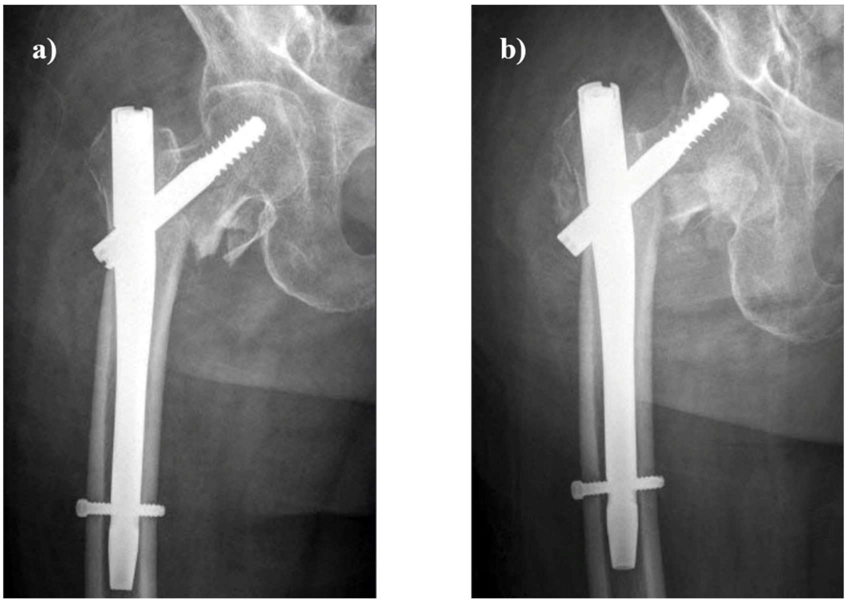

Fig. 1 Intramedullary nail implant as a treatment for the intertrochanteric fracture. a) Immediate postoperative radiography. b) Fixation device failure resulting in cut-out. Modified from [9] (reproduced with editorial permissions).

The incidence of cut-out is high and varies attending to the implant type and the fracture mode [10]. For instance, Caruso *et al*. reported a 5.6% incidence of the cut-out in their study [10], and Tsai *et al*. a 12.5% incidence [11]. In contrast, Van den Brink and Janssen [12] notified an incidence of 0.16% for the mechanical failure. Wadhwani *et al*. also concluded that this phenomenon is the most common among the major complications of these interventions [13].

Numerous studies report on the cut-out phenomenon. The most relevant for this work are those that analyse its incidence [13] or the importance of nail position [14], either clinically [15] or employing numerical finite element models [14][16]. Other authors, such as Lenich *et al*., have developed mechanical systems to reproduce the mechanical behaviour of the femur-nail structure and thus analyse the failure mechanisms that occur on it under fatigue tests [17]. There are also several experimental studies in which the interaction of the trabecular tissue and cephalic screw has been analysed in order to estimate the maximum torque for this fixation [18]–[20]. Although some works focus on this topic, several variables of interest could also be analysed thanks to other experimental techniques (such as digital image correlation) or finite element modelling. For instance, to the authors' knowledge, microrotations between trochanteric area and femoral head or torque have not been analysed in this type of problem. However the torque in the interaction bone-screw has been separately analysed in other experimental works [18]–

[20]. It is crucial to quantify those variables in daily activities in order to improve the mechanical behaviour of the femur-nail structure.

In this work, the cut-out was studied by a combination of experimental testing and finite element modelling. Experimental testing gives a general overview of the mechanical behaviour of the femur-nail setup, helping to understand the mechanical behaviour of the structure under simplified loads and it is helpful for numerical model validation. Numerical models allow the analysis of displacement and stress distributions induced in the femur due to an external load and under more realistic conditions. Numerical models allow to estimate variables and to apply loading conditions that are difficult to study experimentally. In our work, an artificial femur was used to simulate an intertrochanteric fracture and its treatment with an intramedullary nail. This femur simulant simplifies the problem and reduces other potential sources of error. The numerical model of the femur has also been developed to reproduce the loading conditions and estimate the stress state. In addition, damage modelling has been included in our numerical model to predict trabecular bone failure due to critical loads. Simplified experimental tests have been used to validate the numerical model, in which several positions of the intramedullary nail and their effects on the femoral head will be analysed to study the cut-out risk. Stresses in the intramedullary nail, stresses and damage in bone and torque will be related to the risk of failure due to cut-out. This combination of experimental tests and numerical modelling enables the quantification of the cut-out risk through some critical variables studied in this phenomenon.

2. Material and methods.

2.1. Experimental work.

2.1.1. Fracture development and fixation.

In this work, an artificial femur (Model No. 3406, Sawbones, Pacific Research Laboratories Inc., Vashon, USA) (**Fig. 2**a) and an intramedullary nail PFNA (Proximal Femoral Nail Antirotation, Synthes GmbH, Oberdorf, Switzerland) have been used (**Fig. 2**b).

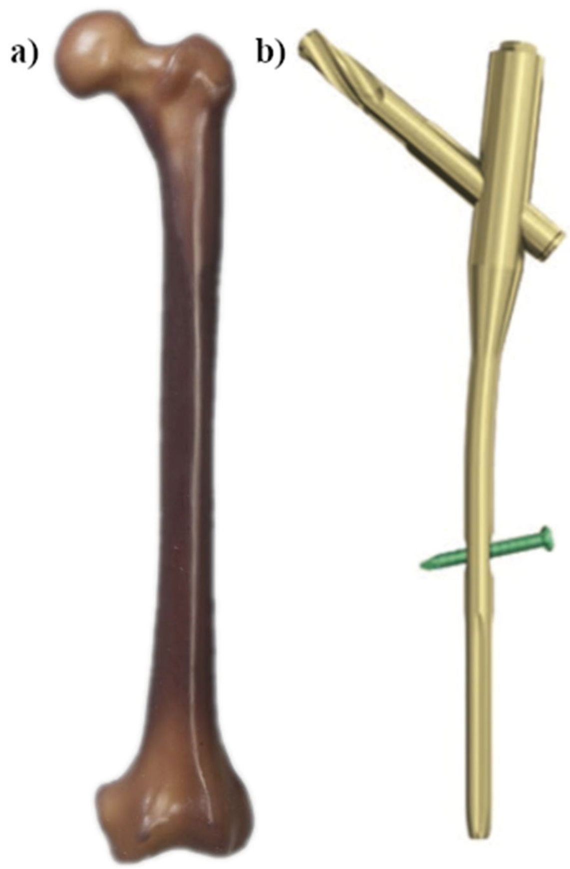

Fig. 2 Specimen used for the experimental work and intramedullary nail. a) Artificial femur Model No. 3406, Sawbones. b) Intramedullary nail PFNA.

An artificial femur was chosen because it is easy to handle and has well-known properties already characterized by several authors, with a mechanical behaviour representative of a common human femur [21]–[23].

2. Material and methods

An intertrochanteric fracture type 31A1, attending to the AO/OTA classification [24] was made in the artificial femur by an experienced trauma surgeon (Dr. Ricardo Larraínzar). This fracture was fixed with the aforementioned intramedullary nail, resulting in a set formed by the fractured femur fixed with the intramedullary nail.

2.1.2. Femur mechanical test.

The main goal of the experimental testing was to validate the numerical model (explained in the next section) and evaluate the rotation of the femoral head around the intramedullary nail.

In the mechanical test, the set formed by the fractured artificial femur and the intramedullary nail (henceforth named as "experimental set") was submitted to static loading (200 N, 400 N, 600 N, 800 N, 1000 N) at 0.5 mm/s speed to keep quasi-static conditions. This test was performed using a universal electromechanical testing machine: Instron 3366 (Instron, Canton, Massachusetts, USA), with a 10 kN load cell.

The measurement of the displacements and strains of the surface of the bone was achieved through the Digital Image Correlation (DIC) technique. This technique was implemented using the software MultiDIC [25] and two digital cameras (Nikon D3300, 24 Megapixels).

The boundary conditions of the experimental test emulated the condition of a person in orthostatic position, as explained below:

- The loads were applied through a rig simulating the contact between the pelvis acetabulum and the femoral head. This condition was implemented using an aluminium tool specifically developed for this purpose and also used in a previous work [26] (**Fig. 3**a). The load was applied with an angle equal to 8º to the vertical line in order to reproduce the actual position of the femur in an orthostatic position [27] (**Fig. 3**b).
- The femur was fixed on its distal region, potting the diaphysis on surgical cement (Surgical Simplex P, STRYKER, Mahwah, NJ, USA) and fixed to the machine using another specially designed aluminium tool (**Fig. 3**a). The testing rig was also used in a previous work by the authors [26].

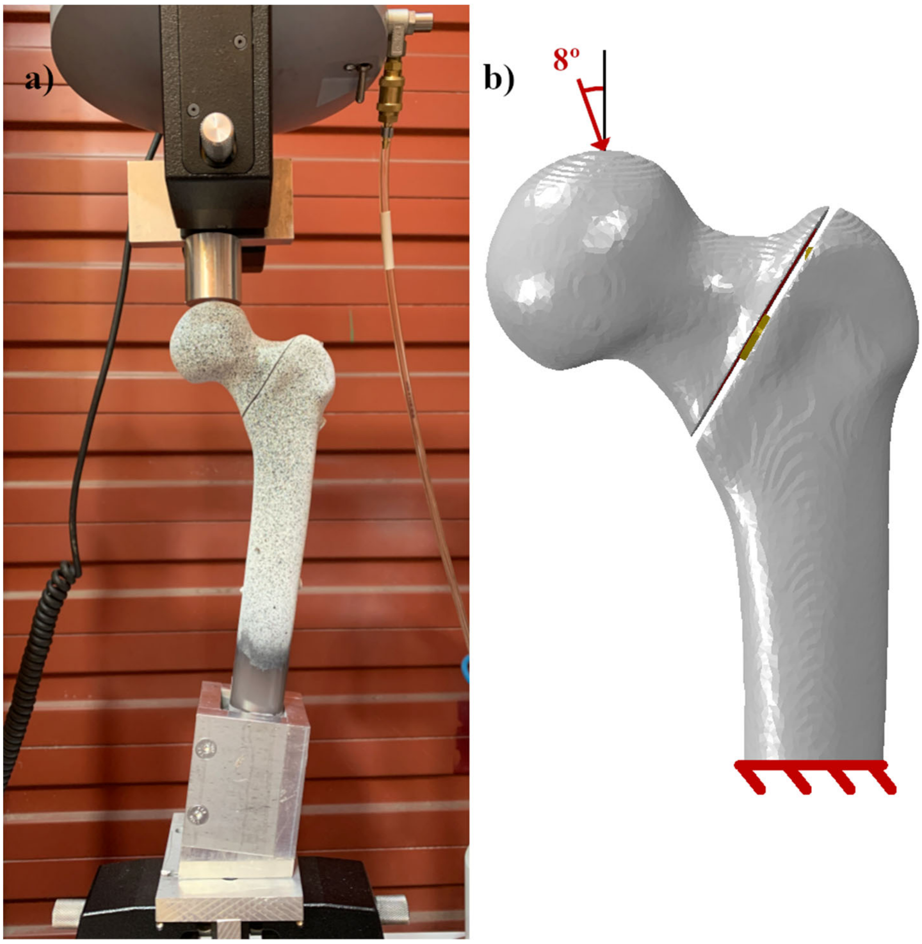

Fig. 3 a) Experimental setup used in the mechanical tests. b) Scheme of the loading conditions reproduced in the mechanical test.

2.2. Finite element model.

The numerical model comprised the same parts as the experimental set (the artificial femur with a 31A1 fracture and the intramedullary nail). The geometries of the entities were digitalized and meshed to reproduce accurately the geometry of the components. The finite element model was developed using Abaqus/Standard.

2.2.1. Obtaining artificial femur geometry from CT scan.

To obtain the geometry of this femur with high resolution, a computerized tomography (CT) was used. The CT scan was performed on a scanner (model Somatom, Siemens Healthcare GmbH, Erlangen, Germany) with a resolution of 0.44 mm in the transverse plane and a thickness of 1 mm in the orthogonal direction. Further treatment of the medical images allowed to generate the geometry of the femur and differentiate cortical and trabecular bone based on the different densities. Subsequently, employing image segmentation and considering the different grayscales (**Fig. 4**a), the geometry shown in **Fig. 4**b was obtained, consisting of the cortical and trabecular tissue.

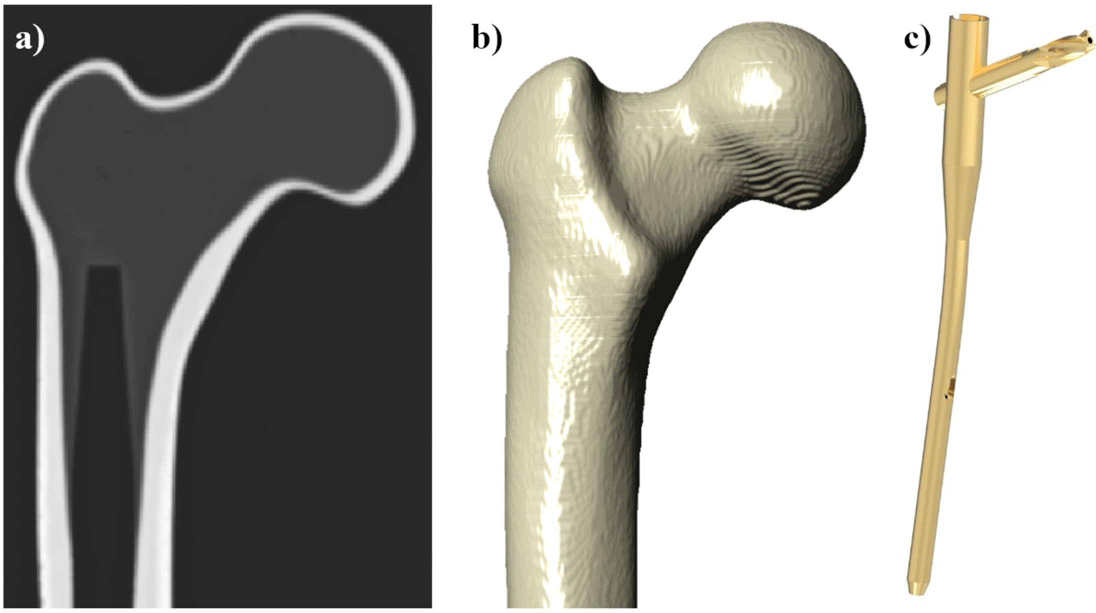

Fig. 4 a) CT scan of the proximal area of the artificial femur before assembling the intramedullary nail. b) Surface geometry obtained from the CT scan. c) Geometric model of the intramedullary nail, rendered image.

2.2.2. Generation of the CAD model of the intramedullary nail.

The geometric model of the intramedullary nail was generated using Solid Edge 2019 software (Siemens PLM, Plano, TX, USA). To this end, the appropriate measurements were taken on the real PFNA-type intramedullary nail to obtain the maximum precision in the geometric model. **Fig. 4**c shows a rendered image from the CAD model of the nail.

2.2.3. Mechanical properties.

Materials involved in the femur are trabecular and cortical artificial bone, besides titanium alloy corresponding to the intramedullary nail, in addition to the aluminium of the mechanical test rig and the surgical cement.

Artificial femur

As previously explained, the artificial femur is made of two well differentiated regions, trabecular bone and cortical bone.

Regarding trabecular tissue, it is a rigid foam with similar properties to those of trabecular bone. It can be considered an isotropic material with homogeneous properties. Moreover, as it will be shown below, damage was simulated in the trabecular tissue using the finite element method, so also degraded properties must be determined. Since compression is the most critical condition for the trabecular bone in our loading simulations, the properties of the finite element will be degraded, simulating bone damage, once the absolute value of the minimum principal stress exceeds the compression strength specified by the manufacturer. This degradation implies a reduction of the stiffness of the damaged elements through a modification of the Young's modulus to a very low value (E=1 MPa). This technique has been used in other works for simulations of bone fracture [28], [29]. Recently, gradient-enhanced damage models have been applied to femur fracture, thanks to the softening phase in the structural response for quasi-brittle materials such as bone [30].

For cortical bone, the manufacturer uses a mixture of short fibreglass and epoxy resin, being in this case a composite material. Since the distribution of the fibres is homogeneous [26], the material was treated as an isotropic material. In this work, damage was not simulated in cortical bone since it is assumed that the cortical bone of the femoral head does not get into contact with the cephalic screw and therefore does not affect the cut-out risk.

Regarding the material model, a linear elastic behaviour was assumed in the artificial femur. Actual human bone presents elastic-plastic behaviour, and some authors have considered this when making numerical models [31], [32]. However, in most cases it is sufficient to analyse the femur as a linear elastic material until failure [31], [33]–[35]. In this case a linear elastic model was deemed valid as relatively low loads are involved. The properties of the artificial femur used in this work were those obtained experimentally by Marco *et al*. [26] and others provided by the manufacturer, as shown in **Table 1**.

Table 1 Mechanical properties of the synthetic femur [26].

	Trabecular bone	Cortical bone
Density, ρ (g/cm^3)	0.27	1.64
Young's modulus, E (MPa)	155	10400
Poisson's ratio, ν	0.30	0.30
Failure stress (compression), σ_c (MPa)	6	157

Intramedullary nail

All the components of the intramedullary nail are made of Ti6Al7Nb [36] alloy, which was modelled as an isotropic material with a linear elastic behaviour up to the elastic limit. The plastic range has not been included in the numerical model since the loading cases are far from inducing plastic deformation in the metallic alloy, which would imply the mechanical failure of the fixation. The properties of this alloy are shown in **Table 2**.

Both parts of the fixation are supposed to be totally coupled in the numerical model, so no glide is allowed between them.

Table 2 Properties of the Ti6Al7Nb alloy [37].

	Ti6Al7Nb
Density, ρ (g/cm^3)	4.52
Young's modulus, E (MPa)	105000
Poisson's ratio, ν	0.36
Yield stress, σ_y (MPa)	900

Testing rig and surgical cement

The mechanical testing rig is made of aluminium modelled as an isotropic material with a linear elastic behaviour. This structure was also included in the model to exactly reproduce the experimental tests. The plastic behaviour has not been considered since the stresses in the tooling were much lower than the aluminium yield stress. The surgical cement has been modelled in the same way. **Table 3** shows the mechanical properties of the aluminium and surgical cement.

Table 3 Properties of aluminium and surgical cement [38].

	Aluminium	Surgical cement
Density, ρ (g/cm^3)	2.70	1.10
Young's modulus, E (MPa)	70	2.40
Poisson's ratio, ν	0.30	0.30

2.2.4. Meshing

The mesh used in the finite element model was formed by quadratic tetrahedral elements (code C3D10 in Abaqus) with an element size of approximately 2 mm, leading to about 280000 element mesh. The size of the element in the intramedullary nail was about 1.5 mm. These element sizes have been established from the experience of previous works [26] and through a mesh sensitivity analysis, reaching minimal variations between consecutive element sizes. **Fig. 5** shows the meshed model of the femur with the intramedullary nail (inside of the femur) and the intertrochanteric fracture.

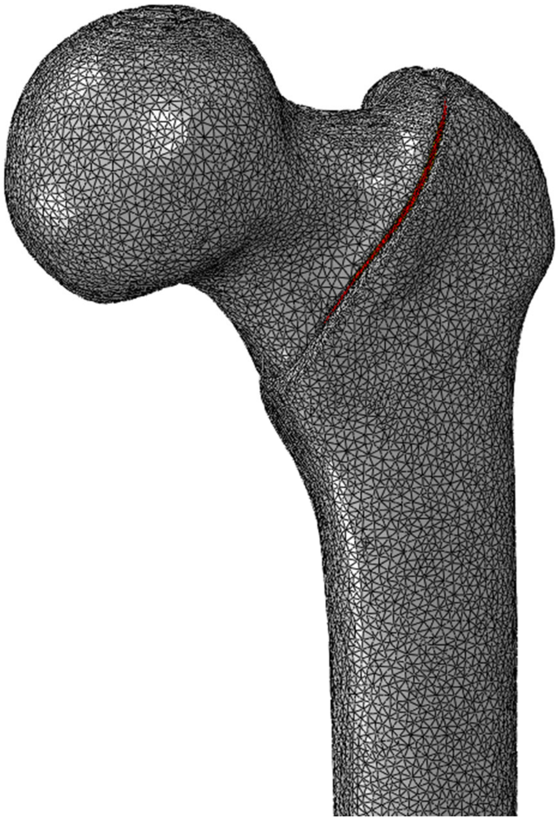

Fig. 5 Numerical model and mesh of the artificial femur and the intramedullary nail. The intertrochanteric fracture can be seen on the bone surface.

2.2.5. Loading conditions.

For the loading conditions, a standard patient of 75 kg has been considered while doing two typical situations from regular life: walking and standing up from a chair.

Standing up from a chair has been chosen as a stance of interest in treating an unstable fracture since some surgeons advise patients not to bear weight during the six weeks after surgery and to follow a sedentary life. The torsional forces on the hip joint when standing up from a chair are very high, making this loading condition critical for this phenomenon. It does not make sense not to allow the patient to walk when the rotational movement of the hip is the most critical and can lead to failure of the fixation. This consideration is clinically relevant and therefore is subjected to analysis in this work.

The data for such cases, i.e. the forces acting on the hip, were obtained from the OrthoLoad database [39]. Specifically, the database from the collection "Standardized Loads Acting in Hip Implants" has been used [40].

Fig. 6 shows the loading cycles for such cases. It is essential to clarify that these loads were not applied through a dynamic model. Instead, 21 load states (each one encompassing 5% of the load cycle) have been obtained from the datasets (for each load scenario), constituting each state a single quasi-static simulation. The load states are performed sequentially. These simulations are not independent in the sense that if certain elements are degraded in one simulation, these elements will remain degraded in the next loading state.

The numerical application of the loads was carried out on a surface which simulates the contact region of the femoral head with the pelvis acetabulum, and the base of the rig support was totally fixed. This contact region is carried out employing a loading reference point coupled to the aforementioned surface, reproducing the experimental test load.

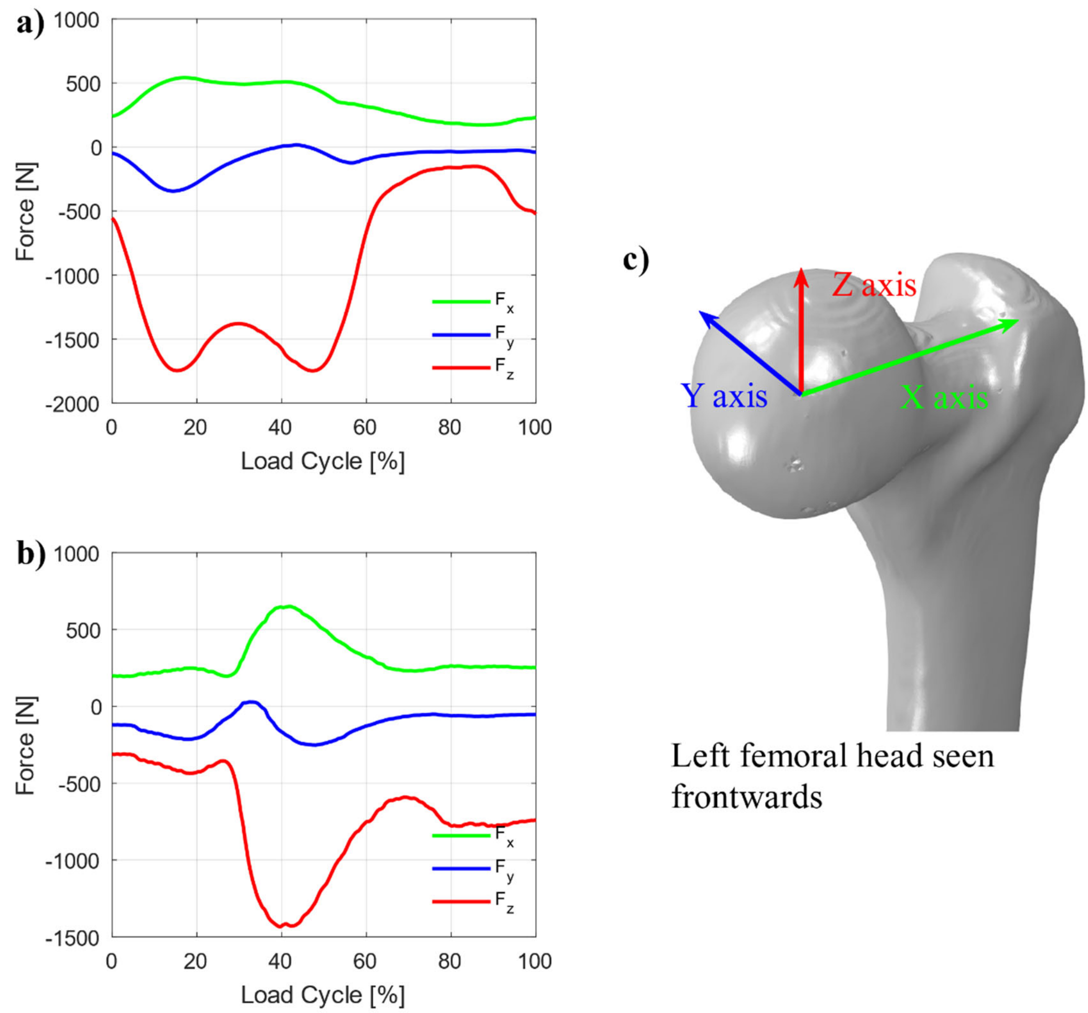

Fig. 6 Applied loads in the numerical model. Data from OrthoLoad collection "Standardized Loads Acting in Hip Implants" [40]. a) Forces acting on the hip for the walking case. b) Forces acting on the hip for the standing-up case. c) Reference system for the forces applied to this model.

2.2.6. Placement of the intramedullary nail in the artificial femur. Study of position influence.

In this work, the influence of the intramedullary nail position was analysed. For this, a central position of the intramedullary nail was used as a reference, and its position was varied ±5 mm in the coronal and sagittal directions (**Fig. 7**). This leads to five configurations under study:

- Reference position: placed in central position with respect to femoral neck section. This location of the intramedullary nail is established as a reference (named as Ref.).
- 5 mm displacement in the sagittal plane posterior direction (named as SagPos5).
- 5 mm displacement in the sagittal plane anterior direction (named as SagAnt5).
- 5 mm displacement in the coronal plane superior direction (named as CorSup5).
- 5 mm displacement in the coronal plane inferior direction (named as CorInf5).

In order to evaluate the failure risk of each position due to cut-out, a radiographic parameter that measures the risk was evaluated. This type of parameters is usually based on geometric measurements that relate the position of the intramedullary nail with respect to the femur. In our case, the Parker parameter [41] was chosen, defined as Parker Ratio (PR):

$$PR = \frac{ab}{ac} \tag{1}$$

where ab and ac are the dimensions shown in **Fig. 8** both in the anteroposterior radiograph (**Fig. 8**a) and in the lateral view (**Fig. 8**b).

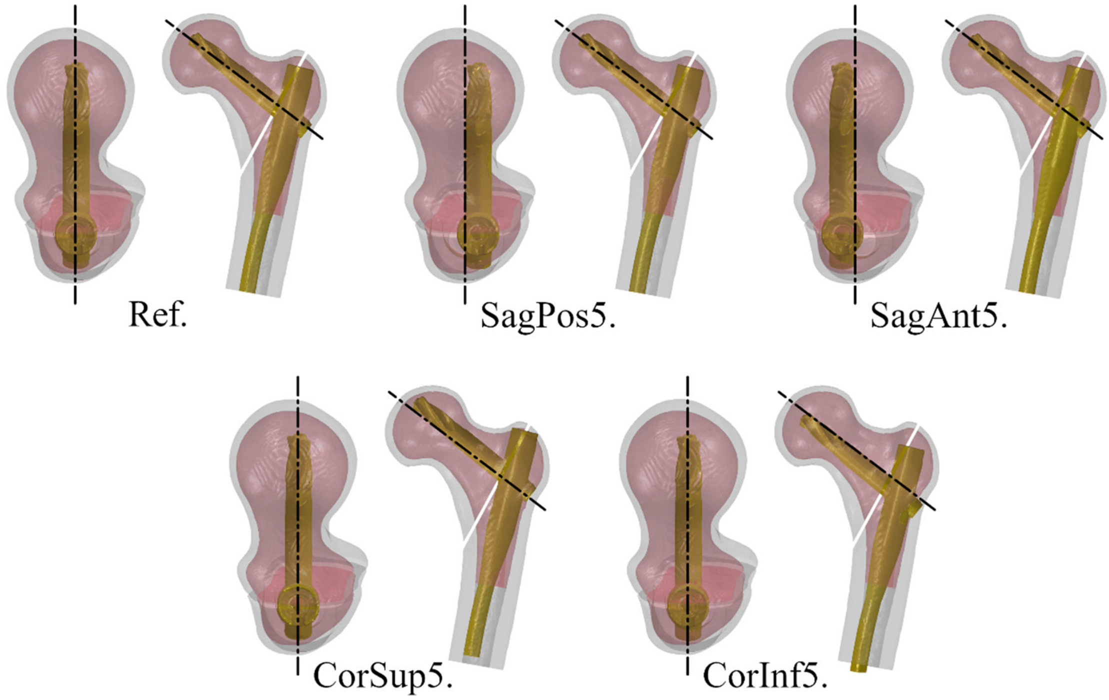

Fig. 7 Positions of the intramedullary nail considered in the study. Trabecular bone tissue is shown in pink, grey cortical bone and gold intramedullary nail. For each of the positions, the transverse view (on the left) and the coronal view (on the right) are shown. Black dashed lines represent the cephalic screw in the reference position.

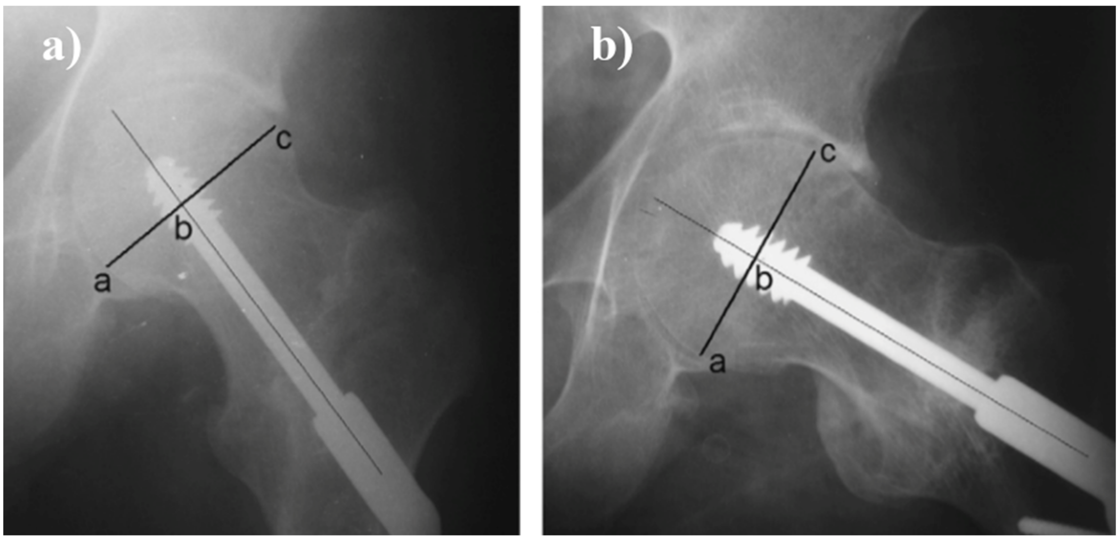

Fig. 8 Radiographs showing the dimensions involved in the calculation of the Parker parameter. Modified from [15]. a) Anteroposterior radiograph. b) Lateral radiograph. (Reproduced with editorial permissions).[1]

[1] Note that in Fig. 8 a sliding hip screw is shown, not an intramedullary nail.

Table 4 shows the Parker parameter values for the positions studied in this work. As can be seen, the reference position shows values close to 50%, while in the other positions the Parker parameters deviate from this value.

Table 4 Parker parameters of the studied positions showed in **Fig. 7**.

Position	Anteroposterior PR [%]	Lateral PR [%]
Ref.	56.8	53.8
SagPos5	55.9	65.4
SagAnt5	56.5	45.5
CorSup5	63.8	57.0
CorInf5	48.0	55.7

It must be established how the values of the Parker parameters affect the cut-out risk. In the original paper, Parker defined this parameter [41]. The established values for the Anteroposterior PR for uneventful events were 45%, whereas the cases with cut-out failure were 58%. For the Lateral PR, these values were 45 % and 36 %, respectively.

Andruszkow *et al*. in [42] analysed the differences between fractures treated with sliding hip screws and intramedullary nails, including different fracture modes according to the AO/OTA classification. In this case, the mean values of 46.47% ± 9.48 for the Anteroposterior PR and 53.38% ± 10.00 for the Lateral PR were obtained for uneventful cases of AO/OTA 31A1 fractures treated with an intramedullary nail. They observed no cases of cut-out failures in this mode of fractures treated with this fixation.

It is also essential to assess how the displacement direction affects the cut-out risk, or, in other words, how changes in Parker parameters affect the cut-out risk. Nevertheless, in this case there is no consensus between different authors. For instance, Parker [41] concluded that there is a cut-out risk increment when the fixation device is displaced towards the posterior direction, i.e. the Lateral PR increases its value. However, Baumgaertner *et al*. [8] announced that cut-out risk increases for anterior displacements, i.e. the Lateral PR decreases its value.

Considering previous papers, the values of 46.47% ± 9.48 for the Anteroposterior PR and 53.38% ± 10.00 for the Lateral PR established by Andruszkow *et al*. in [42] have been set in this work as the reference values for minimum cut-out risk. Hereafter, these values will be considered as “minimal cut-out risk values”. Hence, the closer the Parker ratio to the minimal cut-out risk values, the lower will be considered the cut-out risk.

The variables of interest object of study in this work are:

Von Misses stress in the intramedullary nail

This parameter indicates the stress level due to loading conditions for the fixation device.

Minimal principal stress in the trabecular bone

This variable determines the compression induced in the trabecular bone due to the force exerted by the intramedullary nail. This fact principally occurs in the femoral head, between the external bone surface where the load is applied and the cephalic screw. The higher this value, the higher the possibility of damage in the trabecular bone, leading to slack between the bone and the cephalic screw increasing the cut-out risk.

Volume of damaged trabecular bone

This variable indicates the volume of trabecular tissue where the compression exceeds the critical maximum compression stress in trabecular bone in one loading cycle. This variable is related to the minimal principal stress in the trabecular bone. Once the critical values are exceeded, the trabecular bone is damaged. In the numerical model, this is simulated by the approach of mechanical properties degradation explained in Section 2.2.3.

Torque in the cephalic screw

This is a novel variable that assesses the femoral head and neck's rotation risk in the numerical model. This variable considers the forces acting on the cephalic screw surface as a consequence of the femoral head and neck's action. It calculates the torque produced by the actions of these forces. This variable can be directly related to the cut-out risk since small rotations can reduce the fixation stiffness and damage the tissue, eventually leading to higher rotations and movements of the assembly. For instance, N. Suhm *et al*. [19] experimentally found a significant relationship between torque and cut-out failure.

3. Results

3.1. Experimental results.

3.1.1. DIC software error estimation.

Despite the software MultiDIC has been used in previous works with satisfactory results [25], [43], in this work, an error estimation has been carried out before the definitive DIC tests. The test performed here evaluates the capability of DIC to measure rigid-body displacements with no loads on the specimen. As the influence of speckle size and spacing can be important, this kind of test is necessary to know if the speckle pattern painted on the surface is correctly captured by the system. Reference rigid-body displacements are applied to the specimen, calculating the displacements using the DIC system, similar to the procedure in [44]. For this error estimation, the painted synthetic femur has been subjected to several predefined rigid-body displacements employing the testing machine. Several images have been acquired, and the displacements have been recalculated using MultiDIC. Mean values and standard deviation of the data distribution have been calculated. Hence an error estimation can be performed by comparing the actual displacement and the MultiDIC measurements. Results shown in **Table 5** are very satisfactory, and we conclude that DIC can be applied to our specimen confidently.

Table 5 Results of the MultiDIC software error estimation. Note that Test #1 involves no applied displacement. In this case, two consecutive images were taken of the same static position.

Test #	Applied rigid-body displacement $[mm]$	DIC measured displacement. Mean value $[mm]$	Relative error [%]	Standard deviation $[mm]$
1	0	-0.0026	NaN	0.0006
2	0.1698	0.1659	2.3041	0.0007
3	1.0385	1.0414	0.2824	0.0009
4	5.0186	5.0145	0.0824	0.0029
5	10.0094	10.0054	0.0397	0.0060

3.1.2. Analysis of femoral head rotation.

During the quasi-static experimental test under applied load on orthostatic conditions, any potential femoral head rotation was analysed through displacements obtained on the femoral surface by DIC. Results confirmed that no rotation of the femoral head was observed during the application of loads with the testing machine. A maximum load of

1000 N was applied to the specimen, and there was no relative displacement at both sides of the intertrochanteric fracture of the artificial femur. This reveals that quasi-static loads do not induce a femoral head rotation or sliding; hence the risk of cut-out due to micro displacements is reduced.

3.2. Numerical results.

3.2.1. Numerical model validation.

The numerical model has been validated using the experimental tests and the surface displacements obtained by means of the DIC system. The same loads and conditions have been applied to the numerical model of the synthetic femur, including the aluminium testing rig and surgical cement (section 2.1.2.). At 962 surface points, the magnitude of the displacement vector (total displacement) measured using DIC has been compared to the corresponding numerical prediction at the same points. These points are plotted in **Fig. 9**. The correlation between the experimental and numerical results is reasonable, especially when considering the usual noise of the DIC measurements and the influence of other elements of the testing rig.

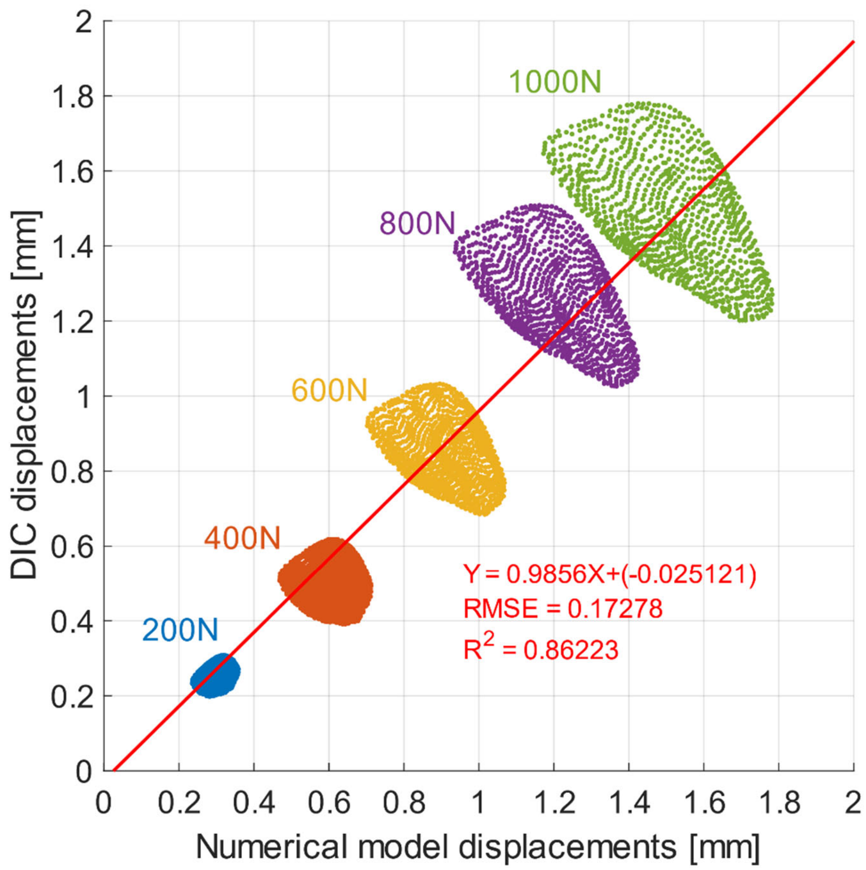

3.Results.

Fig. 9 Comparison between the total displacements measured using DIC in the experimental tests and those obtained with the numerical models at 962 points of the femoral surface. Points for each load are shown in different colours.

3.2.2. Stress in the intramedullary nail.

Table 6 shows the maximum von Mises stress for each nail position analysed. It shows considerable differences in the stress level depending on the intramedullary nail position. Being especially outstanding, the stress increase when the intramedullary nail is displaced through the coronal plane, causing even a risk of plastic strain if exceeding the yield strength of the nail material.

Table 6 Von Mises maximum stress for each studied load. Units in MPa.

	Walking conditions	Standing Up conditions
Ref.	787.7	601.6
SagtPos5	634.9	446.1
SagtAnt5	714.4	499.6
CorSup5	941.7	706.6
CorInf5	1048.9	728.9

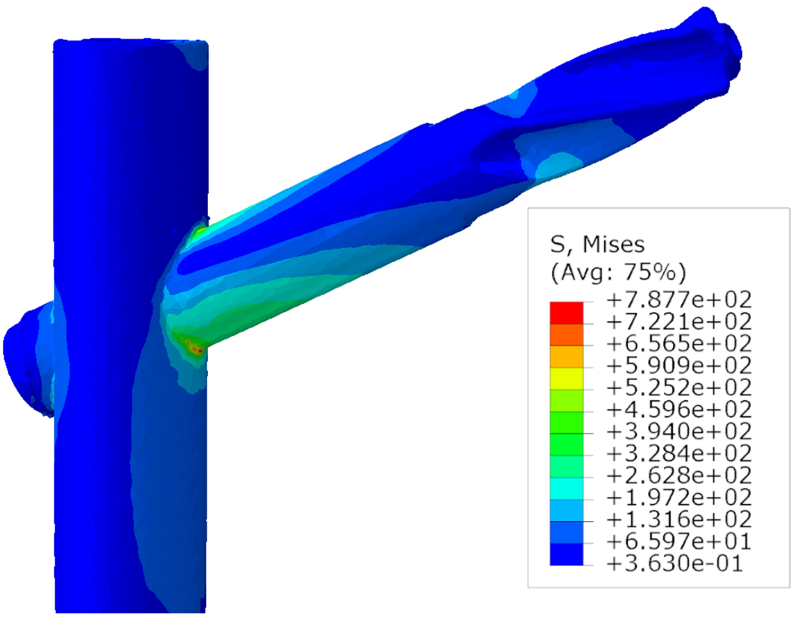

Fig. 10 Example of the von Mises stress distribution in the intramedullary nail on Reference position. Units in MPa.

3.2.3. Torque in the cephalic screw.

Fig. 11 and **Fig. 12** show the torque variations in the cephalic screw for the cases analysed during the simulated cycles, walking and standing up. It is observed that the significant influence on the torque of the displacements through the sagittal plane, leads to values that can be critical for the fixation, as it will be discussed in the next section.

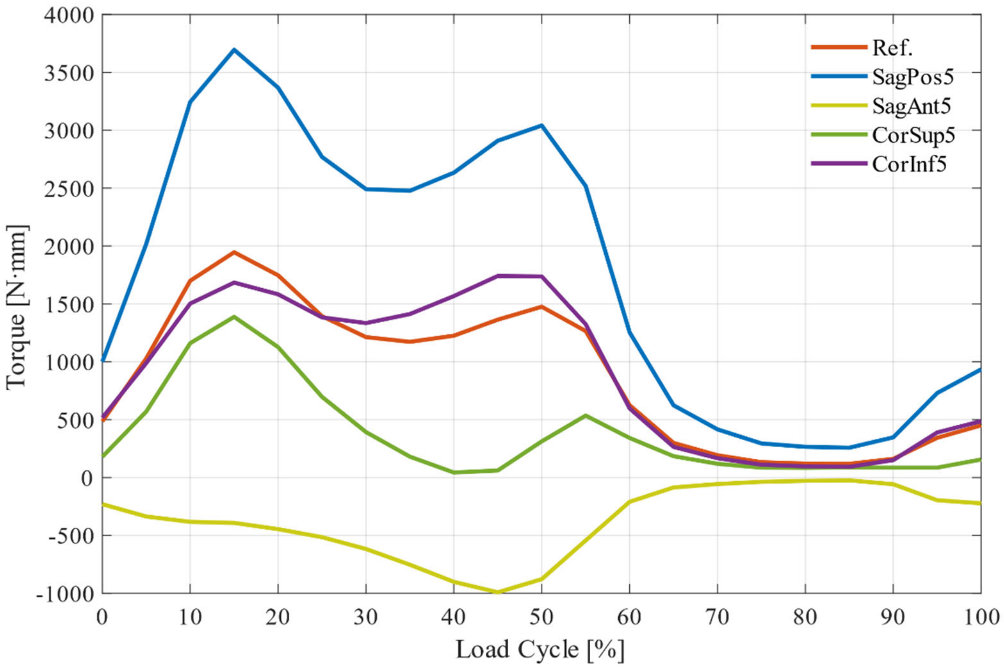

Fig. 11 Torque in the intramedullary nail for the walking load.

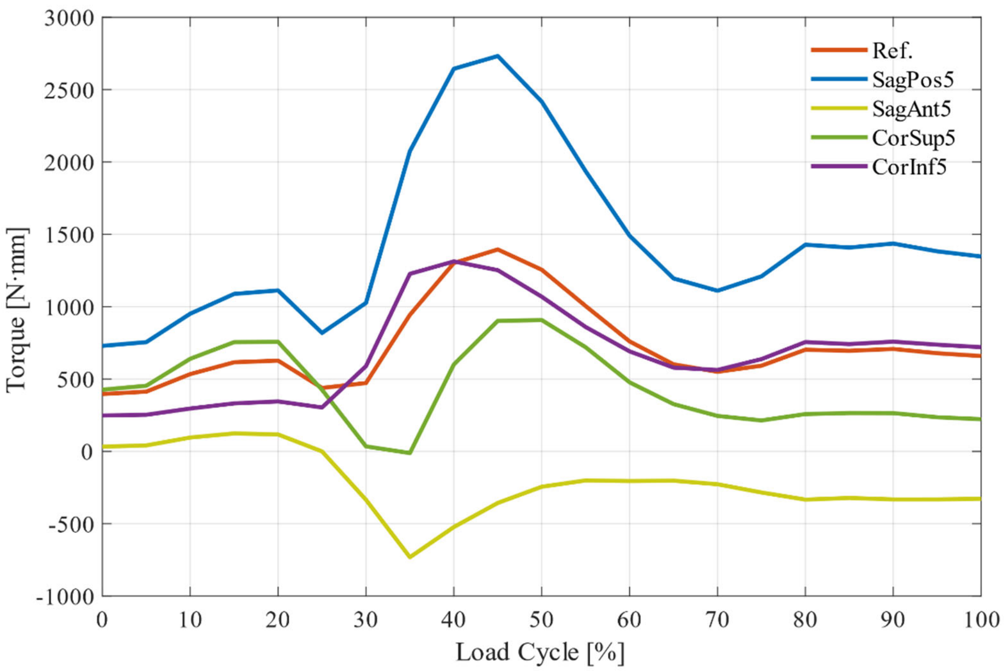

Fig. 12 Torque in the intramedullary nail for the standing-up load.

3.2.4. Minimum principal stress in the trabecular bone of the femoral head.

Table 7 presents the values of minimum principal stress in the trabecular bone of the femoral head for the different load cases. **Fig. 13** shows the contour plot of this stress in the femoral head for the walking load at the most critical point of the load. The contour plots for the Standing-up load are similar. In **Table 7**, it is observed that the CorSup5 presents the highest compression. Concerning the cut-out risk (**Table 4**), this position has the farthest Anteroposterior PR ratio (63.8%) compared to the one of the minimal cut-out risk values. Accordingly, displacements in the superior direction increase the cut-out risk due to the significant compression caused in the trabecular bone of the femoral head, as shown in **Fig. 13.**

Table 7 Minimum principal stresses in the trabecular bone for each studied load case. Units in MPa.

	Walking conditions	Standing up conditions
Ref.	-9.8	-8.5
SagtPos5	-6.0	-5.3
SagtAnt5	-9.7	-7.6
CorSup5	-15.3	-14.0
CorInf5	-10.8	-7.5

Fig. 13 also shows that the area where this significant compression takes place corresponds to the end of the cephalic screw. This compression is especially pronounced when the intramedullary nail is moved upwards in the coronal plane (CorSup5), causing a trabecular tissue thickness reduction between the cephalic screw and the cortical bone. In this case, a reduced bone section resists the same load, leading to higher compressive stresses. Other studies also corroborated this fact, see for instance Goffin *et al.* [43].

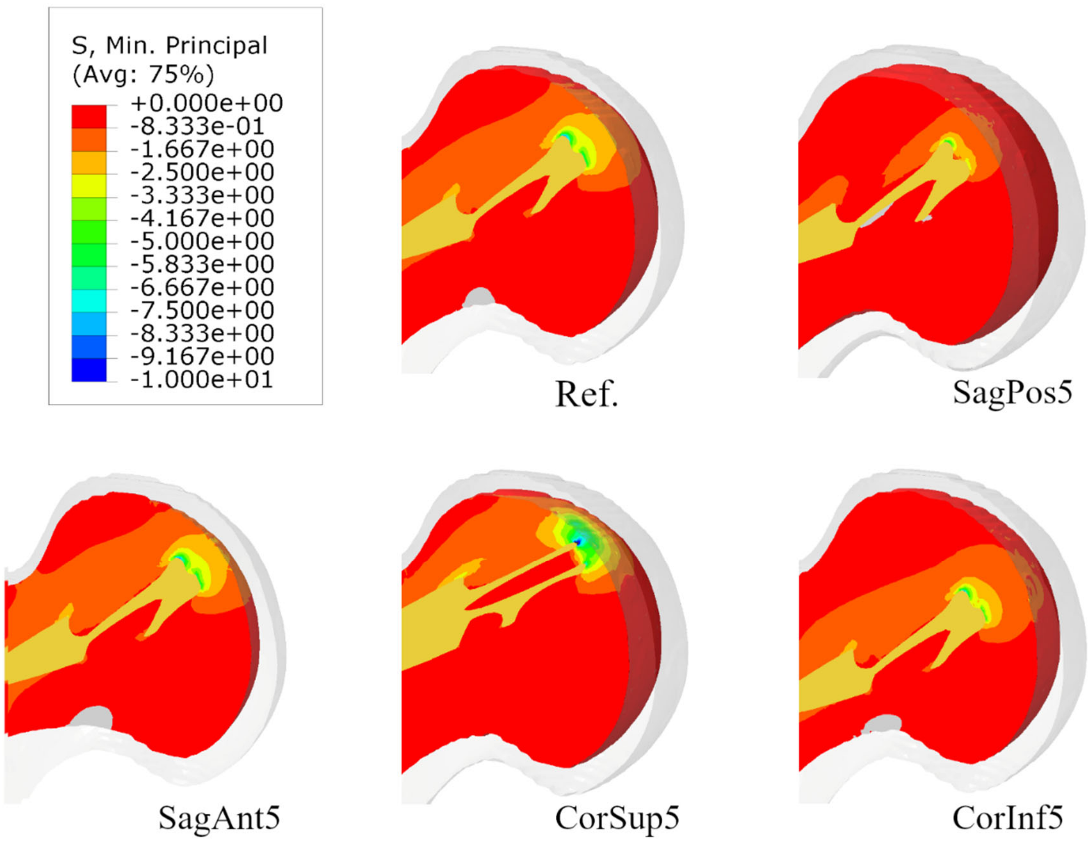

Fig. 13 Minimum principal stresses distribution in the trabecular bone of the femoral head for the walking load case, at the most critical state of load. Units in MPa.

3.2.5. Trabecular bone damage in femoral head.

Fig. 14 and **Fig. 15** show the volume of trabecular bone damaged for the cases analysed in the numerical model during one loading cycle. The trabecular bone damage criterion is based on the minimum principal stress; thus, higher compression results in greater damage in the trabecular bone. The same trends are observed when comparing **Table 7** with **Fig. 14** and **Fig. 15**: the position that increases the compression leads to greater damage in the trabecular bone of the femoral head. Therefore, the cut-out risk associated with displacements in the superior direction is also related to trabecular bone damage of the femoral head.

In contrast, the other positions show a minimal damaged volume of trabecular bone. The compression stresses are insufficient to damage the trabecular bone, and the damaged volume remains almost constant during the cycling load.

Considering these cyclic loads, damaged elements imply the absence of stiffness in the trabecular bone, which can lead to micro-movements in the fixation and screw-bone contact. Finally, after several cycles, this cumulative damage can produce the failure of the set and thus the cut-out phenomenon.

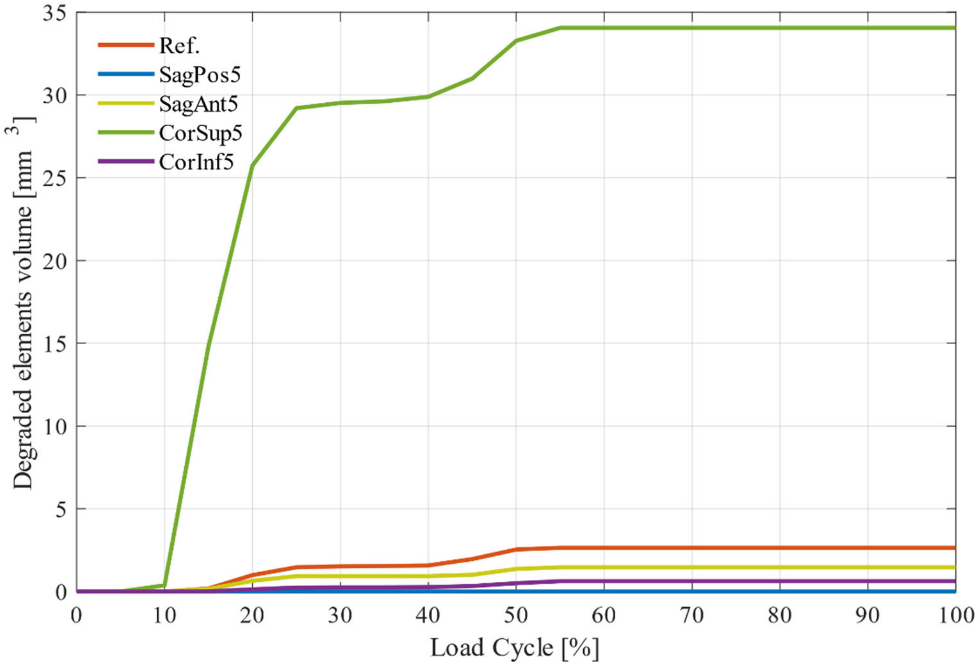

Fig. 14 Damaged volume of trabecular bone for the walking load case.

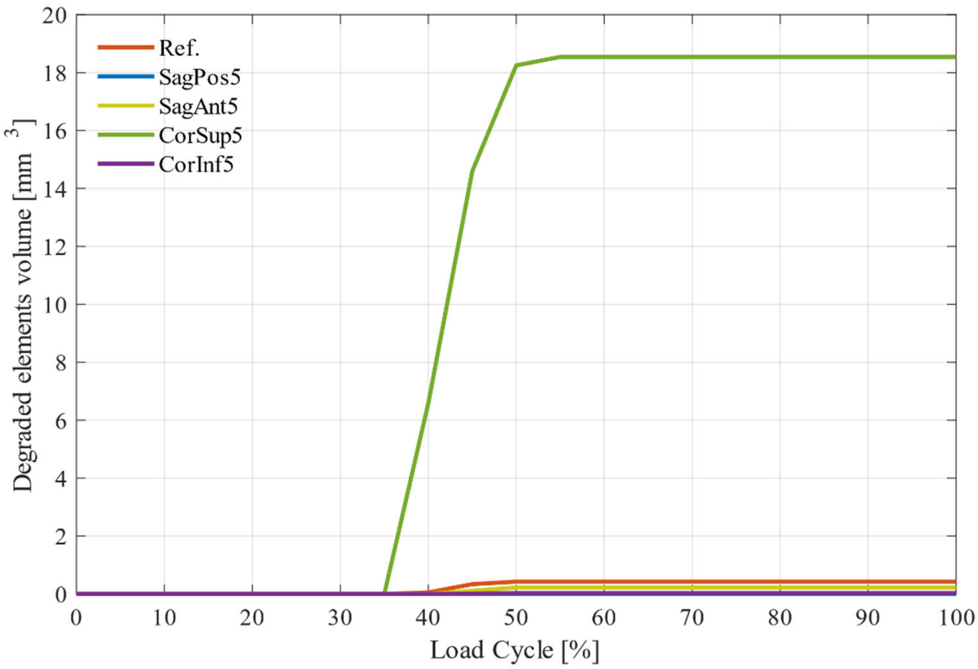

Fig. 15 Damaged volume of trabecular bone for the standing-up load case.

4. Discussion.

This work has been developed with the aim of studying how the position of the intramedullary nail affects the cut-out risk in a proximal femur fracture treatment. For that purpose, a numerical model based on the finite element method has been developed. The numerical model has been validated through experimental tests, obtaining accurate results and enabling the possibility to analyse proper parameters or complex loadings conditions such as daily activities.

Four variables of interest have been measured to assess the cut-out risk. First, regarding the maximum von Mises Stress, the maximum stress is always reached at the same region, i.e., at the union of the cephalic screw and the intramedullary nail (**Fig. 10**). These results agree with Amit Matityahu *et al.* [45]. The maximum stress is due to the stress concentration at this zone and the maximum bending moment generated by the load in this region. Another factor that might contribute to this is the localization of the fracture, which, as can be seen in **Fig. 7**, matches this zone of maximum stress in the screw. As it was observed by Zeng *et al*. [46], this fracture modifies the load transfer, concentrating the stresses around the nail-screw union.

Linking this with the cut-out risk, **Table 6** shows that the CorInf5 position results in the highest stresses. Concerning **Table 4**, this position is shown to be the one with the closer Parker parameters (Anteroposterior PR: 48.0 % and Lateral PR: 55.7%) to the minimal cut-out risk values (Anteroposterior PR: 46.47% ± 9.48 and Lateral PR: 53.38% ± 10.00). Nevertheless, despite this inferior positioning reduces the cut-out risk, which was observed by Quental *et al.* [14], it may endanger the integrity of the intramedullary nail. Similarly, the position CorSup5 also presents high von Mises stresses in the intramedullary nail. On the contrary, both displacements in the sagittal plane tend to reduce the von Mises stress.

The torque in the cephalic screw, as shown in **Fig. 11** and **Fig. 12**, is quite dependent on the displacements through the sagittal plane. This influence is explained by the eccentricity due to the displacements on the sagittal plane with respect to the centre of the femoral head. Note that depending on the displacement direction (posterior or anterior) the torque value is positive or negative, and correspondingly the rotation may tend to occur in one or another direction. **Table 4** shows that the displaced positions over the sagittal plane have the farthest Lateral PR ratios (SagPos5 = 65.4% and SagAnt5 = 45.5%)

to the one of the minimal cut-out risk values. Thus, the displacement in the sagittal plane increases the cut-out risk, which is related to a possible rotation of the femoral head. A clinical statistical study by Bojan *et al.* [47] also observed that the displacements in both anterior and posterior directions increase the cut-out risk. In fact, this study concluded that the correct positioning of the intramedullary nail is a crucial factor in the cut-out risk. Regarding the coronal plane, the superior position of the screw involves a reduction of the torque since the load is applied closer to the cephalic screw, and the angle variations of the load direction have less influence on the mechanical behaviour.

According to results obtained by Gosiewski *et al*. [20] and O'neill *et al*. [18], the maximum torque for this type of fixation is about 2200 N·mm. This value is overcome in SagPos5 for both loading conditions, which would imply rotations that could lead to fixation failure.

This study presents some limitations. First, an artificial femur has been analysed instead of real specimens. Although the human femur would provide more realistic results, an artificial femur permits to isolate the cut-out problem and to analyse critical variables. Real specimens could induce other sources of errors regarding geometry, local material properties variations or local defects. The fracture developed is a simplified morphology and only includes planar surfaces. Moreover, other daily activities could be analysed, but we have focused on daily activities that are more critical for elderly patients. Finally, other variations in the femur-fixation structure could be considered, such as lateral displacements of the femoral head or different fracture morphologies.

5. Conclusions.

In this paper the influence of intramedullary nail position on the cut-out risk has been analysed using numerical modelling and experimental validation on a synthetic bone. The study confirms the centred position as the best for minimum cut-out risk, considering typical cyclic load cases.

The experimental tests provided data for model validation and demonstrated the capability of the MultiDIC software to perform a DIC analysis with good accuracy. In addition, the DIC tests have shown that quasi-static loading conditions do not lead to rotations of the femoral head around the cephalic screw, even for values much higher than average conditions.

The numerical analysis provided several results concerning the cut-out risk:

- Displacements in the lower direction of the coronal plane tend to endanger the fixation device.
- Displacements in the upper direction of the coronal plane increase the cut-out risk, which is related to a compression and trabecular bone damage in the femoral head. However, torque in this position is the lowest in this study.
- Displacements over the sagittal plane also increase the cut-out risk, which is related to a possible rotation in the femoral head. Also, the rotation direction depends on the direction of the displacement.
- Taking all the results globally and considering all the variables analysed in this work, the centred position shows the best performance. Von Mises stresses in the screw are not excessively high, torque is acceptable by the structure, and trabecular bone suffers almost no damage. This result agrees with the dynamic experimental model proposed by Lenich *et al*. [17]. These results could help in the surgery planning with the aim of avoiding damage during service life of the prothesis.

6. Acknowledgments.

The authors gratefully acknowledge the funding support received from the Spanish Ministry of Science and Innovation for funding project PID2020-112628RA-I00/ AEI / 10.13039/501100011033, projects PID2020-118480RB-C21 and -C22 and from the Madrid Community (Spain) through the project IND2020/IND-17413. The financial support of the European Union NextGenerationEU/PRTR through grant number PDC2021-121368-C21 and -C22 and the Generalitat Valenciana through Programme PROMETEO 2021/046 is also acknowledged.

All authors declare that ethical approval was not needed for this work.

All authors declare that they have no conflict of interest.

7. Bibliography.

[1] D. K. Dhanwal, E. M. Dennison, N. C. Harvey, and C. Cooper, "Epidemiology of hip fracture: Worldwide geographic variation.," *Indian J. Orthop.*, vol. 45, no. 1, pp. 15–22, Jan. 2011, doi: 10.4103/0019-5413.73656.

[2] P. Carpintero, J. R. Caeiro, R. Carpintero, A. Morales, S. Silva, and M. Mesa, "Complications of hip fractures: A review," *World J. Orthop.*, vol. 5, no. 4, pp. 402–411, Sep. 2014, doi: 10.5312/wjo.v5.i4.402.

[3] M. Fernández García, J. Martínez, J. M. Olmos, J. González Macías, and J. L. Hernández, "Revisión de la incidencia de la fractura de cadera en España," *Rev. Osteoporos. y Metab. Miner.*, vol. 7, pp. 115–120, 2015, [Online]. Available: http://scielo.isciii.es/scielo.php?script=sci_arttext&pid=S1889-836X2015000400007&nrm=iso.

[4] J. Manninger, U. Bosch, P. Cserháti, K. Fekete, and K. Kazár, *Internal fixation of femoral neck fractures*. 2007.

[5] J. Jacob, A. Desai, and A. Trompeter, "Decision Making in the Management of Extracapsular Fractures of the Proximal Femur - is the Dynamic Hip Screw the Prevailing Gold Standard?," *Open Orthop. J.*, vol. 11, pp. 1213–1217, 2017, doi: 10.2174/1874325001711011213.

[6] A. Pillai, V. Eranki, R. Shenoy, and M. Hadidi, "Age Related Incidence and Early

Outcomes of Hip Fractures: A Prospective Cohort Study of 1177 patients," *J. Orthop. Surg. Res.*, vol. 6, no. 1, p. 5, 2011, doi: 10.1186/1749-799X-6-5.

[7] C. . Wang, C. . Brown, A. . Yettram, and P. Procter, "Intramedullary femoral nails: one or two lag screws? A preliminary study," *Med. Eng. Phys.*, vol. 22, no. 9, pp. 613–624, Nov. 2000, doi: 10.1016/S1350-4533(00)00081-3.

[8] M. R. Baumgaertner, S. L. Curtin, D. M. Lindskog, and J. M. Keggi, "The value of the tip-apex distance in predicting failure of fixation of peritrochanteric fractures of the hip.," *JBJS*, vol. 77, no. 7, 1995, [Online]. Available: https://journals.lww.com/jbjsjournal/Fulltext/1995/07000/The_value_of_the_tip_apex_distance_in_predicting.12.aspx.

[9] S.-R. Lee, S.-T. Kim, M. G. Yoon, M.-S. Moon, and J.-H. Heo, "The Stability Score of the Intramedullary Nailed Intertrochanteric Fractures: Stability of Nailed Fracture and Postoperative Patient Mobilization," *Clin Orthop Surg*, vol. 5, no. 1, pp. 10–18, Mar. 2013, [Online]. Available: https://doi.org/10.4055/cios.2013.5.1.10.

[10] G. Caruso *et al.*, "A six-year retrospective analysis of cut-out risk predictors in cephalomedullary nailing for pertrochanteric fractures: Can the tip-apex distance (TAD) still be considered the best parameter?," *Bone Joint Res.*, vol. 6, no. 8, pp. 481–488, Aug. 2017, doi: 10.1302/2046-3758.68.BJR-2016-0299.R1.

[11] S.-W. Tsai *et al.*, "Risk factors for cut-out failure of Gamma3 nails in treating unstable intertrochanteric fractures: An analysis of 176 patients," *J. Chinese Med. Assoc.*, vol. 80, Jun. 2017, doi: 10.1016/j.jcma.2017.04.007.

[12] W. A. van den Brink and I. M. C. Janssen, "Failure of the Gamma Nail in a Highly Unstable Proximal Femur Fracture: Report of Four Cases Encountered in The Netherlands," *J. Orthop. Trauma*, vol. 9, no. 1, 1995, [Online]. Available: https://journals.lww.com/jorthotrauma/Fulltext/1995/02000/Failure_of_the_Gamma_Nail_in_a_Highly_Unstable.8.aspx.

[13] J. Wadhwani, E. Gil Monzó, J. Pérez Correa, J. García Álvarez, J. Blas Dobón, and J. Rodrigo Pérez, "No todo es 'cut-out': reclasificación de las complicaciones mecánicas del tornillo cefálico del clavo intramedular.," *Rev. Española Cirugía Osteoartic.*, vol. 54, pp. 136–142, 2019, doi: 10.37315/sotocav201928054136.

[14] C. Quental, S. Vasconcelos, J. Folgado, and F. Guerra-Pinto, “Influence of the PFNA screw position on the risk of cut-out in an unstable intertrochanteric fracture: a computational analysis,” *Med. Eng. Phys.*, vol. 97, pp. 70–76, 2021, doi: https://doi.org/10.1016/j.medengphy.2021.10.001.

[15] M. Güven *et al.*, “Importance of screw position in intertrochanteric femoral fractures treated by dynamic hip screw,” *Orthop. Traumatol. Surg. Res.*, vol. 96, no. 1, pp. 21–27, 2010, doi: https://doi.org/10.1016/j.otsr.2009.10.008.

[16] J. M. Goffin, P. Pankaj, and A. H. Simpson, “The importance of lag screw position for the stabilization of trochanteric fractures with a sliding hip screw: A subject-specific finite element study,” *J. Orthop. Res.*, vol. 31, no. 4, pp. 596–600, 2013, doi: 10.1002/jor.22266.

[17] A. Lenich, S. Bachmeier, S. Dendorfer, E. Mayr, M. Nerlich, and B. Füchtmeier, “Development of a test system to analyze different hip fracture osteosyntheses under simulated walking,” *Biomed. Tech.*, vol. 57, no. 2, pp. 113–119, 2012, doi: 10.1515/bmt-2011-0999.

[18] F. O’Neill, F. Condon, T. McGloughlin, B. Lenehan, J. C. Coffey, and M. Walsh, “Dynamic hip screw versus DHS blade,” *J. Bone Joint Surg. Br.*, vol. 93-B, no. 5, pp. 616–621, May 2011, doi: 10.1302/0301-620X.93B5.25539.

[19] N. Suhm, C. Hengg, R. Schwyn, M. Windolf, V. Quarz, and M. Hänni, “Mechanical torque measurement predicts load to implant cut-out: a biomechanical study investigating DHS® anchorage in femoral heads,” *Arch. Orthop. Trauma Surg.*, vol. 127, no. 6, pp. 469–474, 2007, doi: 10.1007/s00402-006-0265-8.

[20] J. D. Gosiewski, T. P. Holsgrove, and H. S. Gill, “The efficacy of rotational control designs in promoting torsional stability of hip fracture fixation,” *Bone Joint Res.*, vol. 6, no. 5, pp. 270–276, May 2017, doi: 10.1302/2046-3758.65.BJR-2017-0287.R1.

[21] B. Pal, S. Gupta, A. M. R. New, and M. Browne, “Strain and Micromotion in Intact and Resurfaced Composite Femurs: Experimental and Numerical Investigations,” *J. Biomech.*, vol. 43, pp. 1923–1930, 2010.

[22] H. Ebrahimi *et al.*, “Biomechanical properties of an intact, injured, repaired, and

healed femur: An experimental and computational study," *J. Mech. Behav. Biomed. Mater.*, vol. 16, pp. 121–135, 2012, doi: https://doi.org/10.1016/j.jmbbm.2012.09.005.

[23] T. Basso, J. Klaksvik, U. Syversen, and O. A. Foss, "A biomechanical comparison of composite femurs and cadaver femurs used in experiments on operated hip fractures," *J. Biomech.*, vol. 47, no. 16, pp. 3898–3902, 2014, doi: https://doi.org/10.1016/j.jbiomech.2014.10.025.

[24] AOTrauma International and Orthopaedic Trauma Association, "Journal of Orthopaedic Trauma - Fracture and Dislocation Classification Compendium," vol. 32, 2018, doi: 10.1097/BOT.0000000000001063.

[25] D. Solav, K. M. Moerman, A. M. Jaeger, K. Genovese, and H. M. Herr, "MultiDIC: An Open-Source Toolbox for Multi-View 3D Digital Image Correlation," *IEEE Access*, vol. 6, pp. 30520–30535, 2018, doi: 10.1109/ACCESS.2018.2843725.

[26] M. Marco, E. Giner, R. Larraínzar-Garijo, J. R. Caeiro, and M. H. Miguélez, "Numerical Modelling of Femur Fracture and Experimental Validation Using Bone Simulant.," *Ann. Biomed. Eng.*, vol. 45, no. 10, pp. 2395–2408, Oct. 2017, doi: 10.1007/s10439-017-1877-6.

[27] L. Cristofolini, E. Schileo, M. Juszczyk, F. Taddei, S. Martelli, and M. Viceconti, "Mechanical testing of bones: the positive synergy of finite-element models and in vitro experiments.," *Philos. Trans. Ser. A, Math. Phys. Eng. Sci.*, vol. 368, no. 1920, pp. 2725–2763, Jun. 2010, doi: 10.1098/rsta.2010.0046.

[28] M. Marco, E. Giner, R. Larraínzar-Garijo, J. R. Caeiro, and M. H. Miguélez, "Modelling of femur fracture using finite element procedures," *Eng. Fract. Mech.*, vol. 196, no. April, pp. 157–167, 2018, doi: 10.1016/j.engfracmech.2018.04.024.

[29] M. Marco, E. Giner, J. R. Caeiro-Rey, M. H. Miguélez, and R. Larraínzar-Garijo, "Numerical modelling of hip fracture patterns in human femur," *Comput. Methods Programs Biomed.*, vol. 173, pp. 67–75, 2019, doi: 10.1016/j.cmpb.2019.03.010.

[30] A. Soni, S. Kumar, and N. Kumar, "Stochastic failure analysis of proximal femur using an isogeometric analysis based nonlocal gradient-enhanced damage model," *Comput. Methods Programs Biomed.*, vol. 220, p. 106820, 2022, doi: https://doi.org/10.1016/j.cmpb.2022.106820.

[31] L. Grassi, S. Väänänen, M. Ristinmaa, J. Jurvelin, and H. Isaksson, "How accurately can subject-specific finite element models predict strains and strength of human femora? Investigation using full-field measurements," *J. Biomech.*, vol. 49, Feb. 2016, doi: 10.1016/j.jbiomech.2016.02.032.

[32] J. H. Keyak and Y. Falkinstein, "Comparison of in situ and in vitro CT scan-based finite element model predictions of proximal femoral fracture load.," *Med. Eng. Phys.*, vol. 25, no. 9, pp. 781–787, Nov. 2003, doi: 10.1016/s1350-4533(03)00081-x.

[33] L. Cristofolini, M. Juszczyk, S. Martelli, F. Taddei, and M. Viceconti, "In vitro replication of spontaneous fractures of the proximal human femur.," *J. Biomech.*, vol. 40, no. 13, pp. 2837–2845, 2007, doi: 10.1016/j.jbiomech.2007.03.015.

[34] M. M. Juszczyk, L. Cristofolini, and M. Viceconti, "The human proximal femur behaves linearly elastic up to failure under physiological loading conditions.," *J. Biomech.*, vol. 44, no. 12, pp. 2259–2266, Aug. 2011, doi: 10.1016/j.jbiomech.2011.05.038.

[35] L. Grassi *et al.*, "Full-field strain measurement during mechanical testing of the human femur at physiologically relevant strain rates.," *J. Biomech. Eng.*, vol. 136, no. 11, Nov. 2014, doi: 10.1115/1.4028415.

[36] Synthes Gmbh, "PFNA. Clavo femoral proximal de antirrotación - Técnica quirúrgica." Oberdorf, Suiza, 2014.

[37] AZO MATERIALS, "Titanium Alloys - Ti6Al7Nb Properties and Applications," 2003. https://www.azom.com/properties.aspx?ArticleID=2064.

[38] J. C. J. Webb and R. F. Spencer, "The role of polymethylmethacrylate bone cement in modern orthopaedic surgery.," *J. Bone Joint Surg. Br.*, vol. 89, no. 7, pp. 851–857, Jul. 2007, doi: 10.1302/0301-620X.89B7.19148.

[39] Julius Wolff Institute, "OrthoLoad," 2021. https://orthoload.com/.

[40] G. Bergmann, A. Bender, J. Dymke, G. Duda, and P. Damm, "Standardized Loads Acting in Hip Implants," *PLoS One*, vol. 11, no. 5, p. e0155612, May 2016, [Online]. Available: https://doi.org/10.1371/journal.pone.0155612.

[41] M. J. Parker, "Cutting-out of the dynamic hip screw related to its position," *J. Bone Joint Surg. Br.*, vol. 74, no. 4, p. 625, 1992, [Online]. Available:

http://europepmc.org/abstract/MED/1624529.

[42] H. Andruszkow *et al.*, “Tip apex distance, hip screw placement, and neck shaft angle as potential risk factors for cut-out failure of hip screws after surgical treatment of intertrochanteric fractures,” *Int. Orthop.*, vol. 36, no. 11, pp. 2347–2354, Nov. 2012, doi: 10.1007/s00264-012-1636-0.

[43] D. Solav, K. M. Moerman, A. M. Jaeger, and H. M. Herr, “A Framework for Measuring the Time-Varying Shape and Full-Field Deformation of Residual Limbs Using 3-D Digital Image Correlation,” *IEEE Trans. Biomed. Eng.*, vol. 66, no. 10, pp. 2740–2752, 2019, doi: 10.1109/TBME.2019.2895283.

[44] M. Palanca, M. Marco, M. L. Ruspi, and L. Cristofolini, “Full-field strain distribution in multi-vertebra spine segments: An in vitro application of digital image correlation,” *Med. Eng. Phys.*, vol. 52, pp. 76–83, 2018, doi: https://doi.org/10.1016/j.medengphy.2017.11.003.

[45] A. Matityahu, A. H. Schmidt, A. Grantz, B. Clawson, M. Marmor, and R. T. McClellan, “The Variable Angle Hip Fracture Nail Relative to the Gamma 3: A Finite Element Analysis Illustrating the Same Stiffness and Fatigue Characteristics,” *Adv. Orthop.*, vol. 2013, p. 143801, 2013, doi: 10.1155/2013/143801.

[46] W. Zeng, Y. Liu, and X. Hou, “Biomechanical evaluation of internal fixation implants for femoral neck fractures: A comparative finite element analysis,” *Comput. Methods Programs Biomed.*, vol. 196, p. 105714, 2020, doi: https://doi.org/10.1016/j.cmpb.2020.105714.

[47] A. Bojan, C. Beimel, G. Taglang, D. Collin, C. Ekholm, and A. Jönsson, “Critical factors in cut-out complication after Gamma Nail treatment of proximal femoral fractures,” *BMC Musculoskelet. Disord.*, vol. 14, p. 1, Jan. 2013, doi: 10.1186/1471-2474-14-1.

[48] J. M. Goffin, P. Pankaj, and A. H. Simpson, “The importance of lag screw position for the stabilization of trochanteric fractures with a sliding hip screw: a subject-specific finite element study.,” *J. Orthop. Res. Off. Publ. Orthop. Res. Soc.*, vol. 31, no. 4, pp. 596–600, Apr. 2013, doi: 10.1002/jor.22266.